A&A 617, L8 (2018)
https://doi.org/10.1051/0004-6361/201834160

Astronomy & Astrophysics

LETTER TO THE EDITOR

NuSTAR and NICER reveal IGR J17591–2342 as a new accreting millisecond X-ray pulsar

A. Sanna[1], C. Ferrigno[2], P. S. Ray[3], L. Ducci[4], G. K. Jaisawal[5], T. Enoto[6,7], E. Bozzo[2], D. Altamirano[8], T. Di Salvo[9], T. E. Strohmayer[10], A. Papitto[11], A. Riggio[1], L. Burderi[1], P. M. Bult[10], S. Bogdanov[12], A. F. Gambino[9], A. Marino[9,13,14], R. Iaria[9], Z. Arzoumanian[10], D. Chakrabarty[15], K. C. Gendreau[10], S. Guillot[16,17], C. Markwardt[10], and M. T. Wolff[3]

[1] Dipartimento di Fisica, Università degli Studi di Cagliari, SP Monserrato-Sestu km 0.7, 09042 Monserrato, Italy
e-mail: andrea.sanna@dsf.unica.it
[2] ISDC, Department of Astronomy, University of Geneva, Chemin d'Écogia 16, 1290 Versoix, Switzerland
[3] Space Science Division, Naval Research Laboratory, Washington, DC 20375-5352, USA
[4] Institut für Astronomie und Astrophysik, Eberhard Karls Universität, Sand 1, 72076 Tübingen, Germany
[5] National Space Institute, Technical University of Denmark, Elektrovej 327-328, 2800 Lyngby, Denmark
[6] Department of Astronomy, Kyoto University, Kitashirakawa-Oiwake-cho, Sakyo-ku, Kyoto, Kyoto 606-8502, Japan
[7] The Hakubi Center for Advanced Research, Kyoto University, Yoshida-Ushinomiya-cho, Sakyo-ku, Kyoto 606-8302, Japan
[8] Physics & Astronomy, University of Southampton, Southampton, Hampshire SO17 1BJ, UK
[9] Università degli Studi di Palermo, Dipartimento di Fisica e Chimica, via Archirafi 36, 90123 Palermo, Italy
[10] Astrophysics Science Division, NASA's Goddard Space Flight Center, Greenbelt, MD 20771, USA
[11] INAF, Osservatorio Astronomico di Roma, Via di Frascati 33, 00044 Monteporzio Catone (Roma), Italy
[12] Columbia Astrophysics Laboratory, Columbia University, 550 West 120th Street, New York, NY 10027, USA
[13] INAF/IASF Palermo, via Ugo La Malfa 153, 90146 Palermo, Italy
[14] IRAP, Université de Toulouse, CNRS, UPS, CNES, Toulouse, France
[15] MIT Kavli Institute for Astrophysics and Space Research, Massachusetts Institute of Technology, Cambridge, MA 02139, USA
[16] CNRS, IRAP, 9 avenue du Colonel Roche, BP 44346, 31028 Toulouse Cedex 4, France
[17] Université de Toulouse, CNES, UPS-OMP, 31028 Toulouse, France

Received 30 August 2018 / Accepted 10 September 2018

ABSTRACT

We report the discovery by the Nuclear Spectroscopic Telescope Array (*NuSTAR*) and the Neutron Star Interior Composition Explorer (NICER) of the accreting millisecond X-ray pulsar IGR J17591–2342. Coherent X-ray pulsations around 527.4 Hz (1.9 ms) with a clear Doppler modulation were detected. This implies an orbital period of ∼8.8 h and a projected semi-major axis of ∼1.23 lt-s. With the binary mass function, we estimate a minimum companion mass of 0.42 $M_{\odot}$, obtained assuming a neutron star mass of 1.4 $M_{\odot}$ and an inclination angle lower than 60°, as suggested by the absence of eclipses or dips in the light curve of the source. The broad-band energy spectrum, obtained by combining *NuSTAR*, *Swift*, and INTEGRAL observations, is dominated by Comptonisation of soft thermal seed photons with a temperature of ∼0.7 keV by electrons heated to 21 keV. We also detect black-body-like thermal direct emission that is compatible with an emission region of a few kilometers and a temperature compatible with the seed source of Comptonisation. A weak Gaussian line centred on the iron Kα complex can be interpreted as a signature of disc reflection. A similar spectrum characterises the NICER spectra, which was measured when the outburst faded.

Key words. accretion, accretion disks – stars: low-mass – pulsars: general – stars: neutron – X-rays: binaries

1. Introduction

Accreting fast-rotating neutron stars (NS) in low-mass X-ray binaries have been investigated for almost two decades. This class of objects, also known as accreting millisecond X-ray pulsars (AMXPs), currently includes 21 sources with spin periods ranging between 1.7 ms and 9.5 ms (see Burderi & Di Salvo 2013; Patruno & Watts 2012; Campana & Di Salvo 2018, for extensive reviews). The characteristic short spin periods observed in AMXPs are the result of long-lasting mass transfer from an evolved sub-solar companion star via Roche-lobe overflow onto a slow-rotating NS (recycling scenario; Alpar et al. 1982), making them the progenitors of rotation-powered millisecond pulsars that emit from the radio to the gamma-ray band. Almost one-third of the AMXPs are ultra-compact binary systems ($P_{\rm orb}$ < 1 h), and the remainder show short orbital periods on average ($P_{\rm orb}$ < 12 h), except for the intermittent pulsar Aql X−1 (Casella et al. 2008), whose period is $P_{\rm orb}$ ∼ 18 h (Welsh et al. 2000). Short orbital periods suggest small, low-mass companion stars, consistent with donor masses of <0.2 $M_{\odot}$ on average.

Here, we report on the detection of millisecond X-ray pulsations from IGR J17591–2342, an X-ray transient that was first detected by the INTernational Gamma-Ray Astrophysics Laboratory (INTEGRAL) during a scan of the Galactic centre on

2018 August 10 (Ducci et al. 2018). An archival search in the *Neil Gehrels Swift* Observatory (*Swift*) Burst Alert Telescope data revealed the source to be active since 2018 July 22 (Krimm et al. 2018). Pointed *Swift*/XRT observations of the source region on 2018 August 12 revealed a point-like X-ray source and determined its precise X-ray position (Bozzo et al. 2018), which was refined by a *Chandra* observation on 2018 August 23 to be RA = $17^{\rm h}59^{\rm m}02.83^{\rm s}$ Dec = $-23°43'10.2''$ (J2000) with an astrometric uncertainty of 0.6″ (Nowak et al. 2018). On 2018 August 14, the Australia Telescope Compact Array (ATCA) detected IGR J17591–2342 with a flux density $S_\nu = 1.09 \pm 0.02$ mJy and $S_\nu = 1.14 \pm 0.02$ mJy (at 68% c.l.) at 5.5 GHz and 9.0 GHz, respectively, at a position RA = $17^{\rm h}59^{\rm m}$ $02.83^{\rm s} \pm 0.04^{\rm s}$ Dec = $-23°43'08.3'' \pm 0.1''$. This is consistent with the X-ray determinations (Russell et al. 2018).

In this Letter, we describe a coherent timing analysis of the Nuclear Spectroscopic Telescope Array (*NuSTAR*) and Neutron Star Interior Composition Explorer (NICER) observations that provided the pulsar spin period and binary ephemeris. We also analyse the X-ray spectral modelling obtained from *NuSTAR*, *Swift*, INTEGRAL, and NICER data.

2. Observations and data reduction

IGR J17591–2342 was observed by IBIS/ISGRI on board the INTEGRAL satellite from 2018 August 10 at 15:50 to August 11 at 12:30 UT for a total exposure time of 66 ks. We performed the data reduction and analysis using the off-line science analysis (OSA) software provided by the INTEGRAL Science Data Centre. We produced a mosaic image from the combined individual images of the available data set, where the source was detected with a significance $>7\sigma$ in the 20–80 keV energy band. We extracted the average IBIS/ISGRI spectrum in 8 bins from 25 to 150 keV with equal logarithmic spacing. No JEM-X data were available because the source is located at the edge of its field of view.

NuSTAR observed IGR J17591–2342 (Obs.ID. 90401331002) on 2018 August 13 starting from 22:36 UT for a total exposure of ∼30 ks. We performed standard screening and filtering of the events using the *NuSTAR* data analysis software (NUSTARDAS) from HEASOFT version 6.24. We extracted source events from a circular region of radius 80″ centred on the source position. We extracted the background with a similar extraction area, but located in a region far from the source with similar degree of straylight contamination. The average source count rate per instrument is ∼9 counts s^{-1} in the energy range 3–80 keV. We corrected for spacecraft clock drift by applying the latest clock correction file (version 84, valid up to 2018-08-14).

Swift observed IGR J17591–2342 (Obs.ID. 00010804002) on 2018 August 14 from 00:38 UT for a total of ∼0.6 ks with *Swift*/XRT operated in photon-counting mode. We reduced and processed the XRT data with XRTPIPELINE version 0.13.4, extracting source events from a circular region of radius 64″. We estimated a source count rate of ∼1 counts s^{-1} above the pile-up threshold (see, e.g. Romano et al. 2006). Thus, we extracted the source spectrum using an annular region centred at the source position with inner and outer radius of 10″ and 64″, respectively. Similarly, we extracted the background spectrum from an annular region with inner and outer radius of 102″ and 230″, respectively.

NICER observed IGR J17591–2342 on 2018 August 15 from 00:00 to 14:08 UT for a total exposure of ∼7.3 ks (Obs.ID. 1200310101, hereafter NICER-1), on August 18 from 02:08 to 03:56 UT (exposure of ∼1.5 ks, Obs.ID. 1200310102, NICER-2), on August 23 from 00:58 to 22:57 UT (exposure of ∼11.5 ks, Obs.ID. 1200310103, NICER-3), and on August 24 from 01:51 to 14:44 UT (exposure of ∼7 ks, Obs.ID. 1200310104, NICER-4). We filtered events in the 1–12 keV band applying standard screening criteria with NICERDAS version 4.0. We removed short intervals that showed background flaring in high geomagnetic latitude regions. The spectral background was obtained from blank-sky exposures.

We did not detect any Type-I thermonuclear burst during the observations analysed in this work.

Table 1. Orbital parameters and spin frequency of IGR J17591–2342 with uncertainties on the last digit quoted at 1σ confidence level.

Parameters	*NuSTAR*	NICER	*NuSTAR* + NICER
RA[a] (J2000)		$17^{\rm h}59^{\rm m}02.86^{\rm s} \pm 0.04^{\rm s}$	
Dec[a] (J2000)		$-23°43'08.3'' \pm 0.1''$	
$P_{\rm orb}$ (s)	31684.8 ± 0.1	31684.743 ± 0.003	31684.738 ± 0.002
x (lt-s)	$1.22774 \pm 1 \times 10^{-5}$	$1.227716 \pm 8 \times 10^{-6}$	$1.227728 \pm 7 \times 10^{-6}$
$T_{\rm NOD}$ (MJD)	$58345.171984 \pm 4 \times 10^{-6}$	$58345.1719787 \pm 16 \times 10^{-7}$	$58345.1719786 \pm 14 \times 10^{-7}$
e	$<1 \times 10^{-4}$	$<6 \times 10^{-5}$	$<5.5 \times 10^{-5}$
ν_0 (Hz)	$527.425790 \pm 1 \times 10^{-6}$	$527.42570042 \pm 8 \times 10^{-8}$	–
$\dot{\nu}$ (Hz s^{-1})	[b]$(2.6 \pm 0.3) \times 10^{-10}$	$(2.0 \pm 1.6) \times 10^{-13}$	–
T_0 (MJD)	58344.0	58344.0	58344.0
$\chi^2_{\rm red}$/d.o.f.	2.27/65	1.25/99	1.67/177

Notes. [a]Localisation of the ATCA radio counterpart (Russell et al. 2018). [b]The spin frequency derivative likely originates from the time drift of the internal clock of the *NuSTAR* instrument, see Sect. 4 for more details. T_0 represents the reference epoch for these timing solutions. Frequencies and times reported here are given in the TDB timescale.

3. Results

3.1. Timing analysis

To search for coherent signals, we first corrected the NICER and *NuSTAR* photon arrival times to the solar system barycentre with the tool BARYCORR, using the DE-405 solar planetary ephemeris, and adopting the source coordinates of Table 1. Power density spectra (PDS) obtained by averaging either *NuSTAR* or NICER 150 s data segments showed a prominent ($>4\sigma$) excess at a frequency of 527.3 Hz. The feature exhibited a double-peaked structure characteristic of orbital Doppler broadening. Inspection of the *NuSTAR* PDS over short segments (500 s) revealed pulse frequency modulation typical for pulsars in binary systems (see Fig. 1). The best fit is found for orbital period $P_{\rm orb} = 31694(67)$ s, projected semi-major axis of the NS orbit $x = 1.233(9)$ lt-s, time of passage through the ascending node $T_{\rm NOD} = 58343.704(1)$ (MJD), and spin frequency $\nu_0 = 527.4253(6)$ Hz.

Starting from this provisional solution, we folded data segments of ∼400 s and ∼300 s for the *NuSTAR* and NICER observations, respectively, into eight phase bins at the preliminary spin frequency ν_0. We modelled each pulse profile with a constant plus two sinusoidal functions, representing the pulse frequency and its second harmonic. We retained only profiles for which the ratio between the pulse frequency amplitude and its 1σ uncertainty was higher than three. We modelled the pulse phase with a linearly varying frequency plus a circular Keplerian orbital model separately for *NuSTAR* and NICER. A more detailed description of the procedure can be found in Sanna et al. (2016, and references therein).

The best-fit orbital and pulsar spin parameters for the *NuSTAR* and NICER data sets are shown in the first and

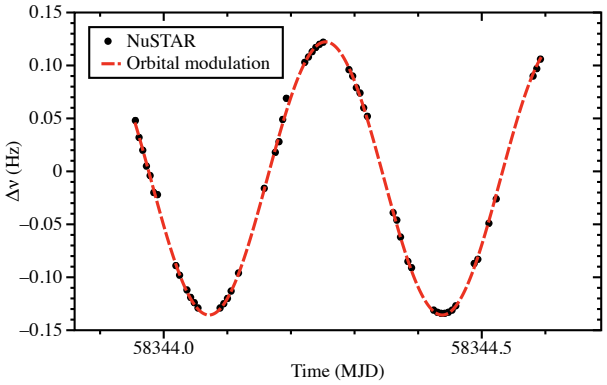

Fig. 1. Time evolution of the pulsar frequency shifts (with respect to $\nu = 527.432$ Hz) estimated from 500 s *NuSTAR* data segments. The frequency shifts show a clear modulation that is compatible with Doppler shifts caused by orbital motion in a binary system. The red dashed line represents the best-fitting orbital Doppler modulation model assuming a circular orbit.

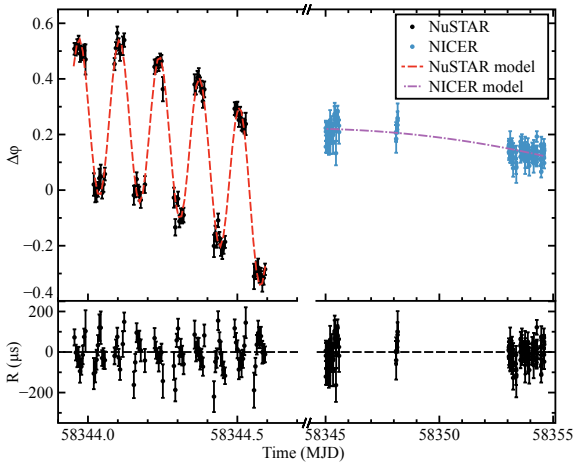

Fig. 2. *Top panel*: pulse phase delays as a function of time computed by epoch-folding at a constant frequency ~400 s and 300 s data intervals of the *NuSTAR* (left) and the NICER (right) data sets, respectively, after correcting for the best orbital solution. In the same panel we show the best-fit models for each group of data. *Bottom panel*: residuals in μs with respect to the best-fitting models for the pulse phase delays.

second column of Table 1, respectively. They are derived from the phase delays at the fundamental frequency; a timing analysis using the second harmonic yields compatible results. The top panel of Fig. 2 shows the *NuSTAR* and NICER pulse phases after correcting for the best orbital solution and assuming a constant frequency. The *NuSTAR* pulse phases show a large distribution of residuals, which is not compatible with the binary orbital modulation. These can be well described (see residuals in the bottom left panel of Fig. 2) by a strong spin frequency derivative (see Table 1) and an additional sinusoidal term with period $P \sim 193$ minutes (close to twice the *NuSTAR* orbital period). We note that no sinusoidal modulation is present in either NICER data (both harmonics) or the *NuSTAR* second harmonic pulse phases, suggesting a likely instrumental origin. For the latter, we emphasise that the phase variations of ~0.5 observed for the fundamental component are close to a complete cycle of the harmonic, tuning down any effect of the phase drift. We also note that the lower statistics in the harmonic would make residuals less evident with respect to the fundamental component.

The NICER pulse phase residuals (top right panel) show a hint of a positive spin frequency derivative (see Table 1 for the corresponding value and the bottom right panel of Fig. 2 for final residuals that account for this component). We improved the orbital parameter estimates (third column of Table 1) by orbitally phase-connecting the available data sets (see, e.g. Sanna et al. 2017a,c, for more details on the procedure). We note that the uncertainty on the source localisation has an effect on the determination of the frequency and frequency derivative, which is more than one order of magnitude smaller than the uncertainties reported in Table 1 for the corresponding parameters. Therefore we ignore this effect.

Finally, we created pulse profiles by epoch-folding the *NuSTAR* (3–80 keV) and NICER (1–12 keV) observations with the parameters reported in Table 1. We modelled them with a combination of three sinusoidal components (see Fig. 3). In *NuSTAR* data, the fundamental, second, and third harmonics have fractional amplitudes of $(16.1 \pm 0.3)\%$, $(5.1 \pm 0.3)\%$, and $(1.5 \pm 0.3)\%$, respectively. NICER pulse profiles are characterised by fractional amplitudes of $(13.7 \pm 0.2)\%$, $(5.0 \pm 0.2)\%$, and $(1.0 \pm 0.2)\%$ for the fundamental, second, and third harmonics, respectively.

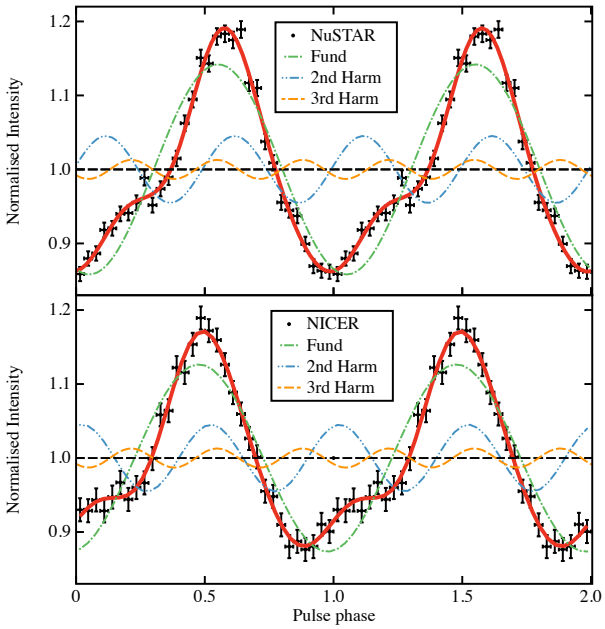

Fig. 3. IGR J17591–2342 pulse profiles (black points) from epoch-folding the *NuSTAR* (*top panel*) and the NICER (*bottom panel*) observations after correcting for the orbital parameters reported in Table 1. The best-fitting model (red line) is the superposition of three sinusoidal functions with harmonically related periods. For clarity, we show two cycles of the pulse profile.

3.2. Spectral analysis

We performed a spectral analysis with Xspec 12.10.0c (Arnaud 1996) after applying an optimal binning (Kaastra & Bleeker 2016). For the first epoch, we used the 0.5–7.5 keV range for *Swift*/XRT, 3–70 keV for *NuSTAR* and 30–80 keV for *IBIS/ISGRI* and grouped the spectra to collect at least 20 counts per bin (Fig. 4). The broad-band (0.5–80 keV) spectrum is well described by an absorbed thermal component (blackbody) with temperature $kT_{\rm BB}$ that also provides the seed photons for a thermally Comptonised continuum with electron energy $kT_{\rm e}$ and a weak emission line centred on the iron Kα

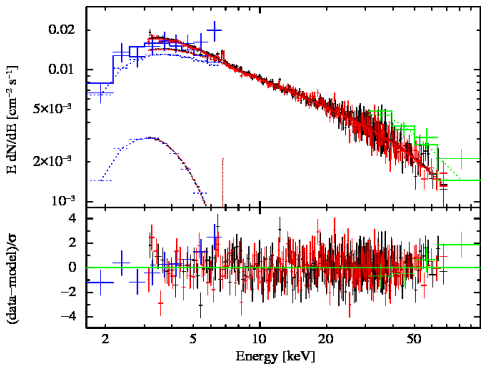

Fig. 4. *Upper panel*: *Swift* (blue), *NuSTAR* FPMA and FPMB (black and red, respectively) and *IBIS/ISGRI* (green) unfolded spectra of IGR J17591–2342. The dashed and dash-dotted lines represent blackbody and Comptonisation components, respectively. The sharp dotted line is a Gaussian with width set to zero. Additional rebinning is for displaying purposes. *Lower panel*: residuals from the best-fit model in units of standard deviations.

complex and width fixed to zero. In Xspec, this is implemented as `TBabs*[cflux*nthcomp+bbodyrad]+gauss`. For the modelling, we left the flux of the Comptonisation component free to vary independently for each instrument to account for cross-instrument calibration offsets and possible source variations that are due to not strictly simultaneous observations.

The NICER observations were fitted independently by minimising the `pgstat` statistic in Xspec[1]. Because of uncertainties in the low-energy response, we ignored the NICER data below 1.4 keV. We adopted the same model, but fixed the electron temperature at the value found from *NuSTAR* and checked that the result remained insensitive as long as $kT_e > 12$ keV. After verifying the compatibility of single spectra, we performed a joint fit of NICER-1 and -2 observations, leaving only the flux to be independently determined between them. We applied the same procedure to NICER-3 and -4. The best-fit parameters are shown in Table 2 with uncertainties at the 90% confidence level. Regardless of the statistical test used to determine the best-fit parameters, we report the χ^2_{red} value.

4. Discussion

We reported the newly discovered AMXP IGR J17591–2342, for which we detected coherent X-ray pulsations at ~527 Hz in the *NuSTAR* and NICER observations performed almost 25 days from the beginning of the outburst, with a pulse fraction of 15%. We modelled the NS spin frequency drift as the Doppler shift induced by the binary orbital motion, discovering the binary nature of the system, which is characterised by an orbital period of almost 8.8 h, very similar to the intermittent AMXP SAX J1748.9−2021 (see, e.g. Altamirano et al. 2008; Sanna et al. 2016) and the eclipsing AMXP SWIFT J1749.4−2807 (see, e.g. Markwardt & Strohmayer 2010; Altamirano et al. 2011; Ferrigno et al. 2011).

The analysis of the *NuSTAR* pulse phase residuals revealed a large spin-up derivative (2.6×10^{-10} Hz s^{-1}) and an oscillation close to twice the satellite orbital period. We suggest that both effects are associated with the time drift of the internal clock instrument (see, e.g. Madsen et al. 2015). Similar spurious

[1] `pgstat` is suited for Poisson distributed data with Gaussian distributed background; see https://heasarc.gsfc.nasa.gov/xanadu/xspec/manual/XSappendixStatistics.html.

Table 2. Best-fit spectral parameters of IGR J17591–2342 with uncertainties at the 90% confidence level.

Parameter	Multiple[a]	NICER-1,2[a]	NICER-3,4[a]
N_H (10^{22}cm^{-2})	3.6 ± 1.1	$3.45^{+0.18}_{-0.15}$	$3.59^{+0.05}_{-0.08}$
Γ	1.76 ± 0.02	1.83 ± 0.06	2.23 ± 0.05
kT_e (keV)	22^{+4}_{-3}	22(fixed)	22(fixed)
kT_{BB} (keV)	0.79 ± 0.09	$0.58^{+0.05}_{-0.07}$	$0.90^{+0.07}_{-0.06}$
r_{bb} (km/D$_{10\,kpc}$)^2	$2.6^{+1.4}_{-0.6}$	$3.3^{+0.8}_{-0.6}$	$<5 \times 10^3$
E_{Fe} (keV)	$6.82^{+0.14}_{-0.39}$	6.35 ± 0.04	6.37 ± 0.10
N_{Fe} (10^{-5} ph s^{-1} cm^{-2})	5.2 ± 1.8	3.8 ± 0.9	2.9 ± 1.6
Flux (1–10 keV)[b]	[c]2.0 ± 0.3	[d]1.85 ± 0.09	[e]$2.35^{+0.03}_{-0.04}$
		[d]$1.06^{+0.08}_{-0.09}$	[e]$2.42^{+0.02}_{-0.04}$
Flux (3–20 keV)[b]	2.41 ± 0.05	–	–
Flux (20–100 keV)[b]	$3.8^{+0.4}_{-0.5}$	–	–
Flux (0.1–10 keV)[f]	1.73	1.31[d]	1.57[e]
		0.78[d]	1.61[e]
χ^2_{red}/d.o.f.	1.09/473	1.11/377	1.13/1129

Notes. [(a)]"Multiple" indicates the combined fit of the *NuSTAR*, *IBIS/ISGRI*, and *Swift*/XRT observations. NICER-1 and NICER-1,2 are the observations of 2018, August 15 and 18, and NICER-3,4 of August 23 and 24. [(b)]The flux of the `nthComp` component is in units of 10^{-10} erg s^{-1} cm^{-2}. The 3–20 and 20–100 keV `nthcomp` fluxes apply to *NuSTAR* and *IBIS/ISGRI* data, respectively. *IBIS/ISGRI* flux is higher than the others, since the data were obtained earlier, when the source was brighter. [(c)]This flux applies to *Swift*/XRT data only. [(d)]The upper and lower rows refer to the NICER-1 and 2 observations. [(e)]The upper and lower rows refer to the NICER-3 and 4 observations. [(f)]Extrapolated absorbed flux derived by the model in units of 10^{-10} erg s^{-1} cm^{-2}. For the multiple observation, we extrapolated the *NuSTAR* spectrum.

frequency derivatives have been reported for *NuSTAR* observations of AMXPs such as MAXI J0911−655 (Sanna et al. 2017b), SAX J1808.4−3658 (Sanna et al. 2017a), and IGR J00291+5934 (Sanna et al. 2017c). The large discrepancy on the spin frequency ((~1×10^{-4} Hz) between *NuSTAR* and NICER is also a direct consequence of the *NuSTAR* clock issue. These considerations are reinforced by the analysis of NICER observations, which do not show any significant frequency drift.

A spin-up frequency derivative of $(2.0 \pm 1.6) \times 10^{-13}$ Hz/s is observed from the phase-coherent timing analysis of the NICER observations. For a broad-band (0.1–100 keV) absorbed flux of $\sim 7 \times 10^{-10}$ erg/s/cm^2 and a source distance of 8.5 kpc (assumed near the Galactic centre, see, e.g. Kerr & Lynden-Bell 1986), we estimate an accretion rate of $\dot{M} \simeq 5.2 \times 10^{-10}\ M_\odot$/yr (for an NS radius and mass of 1.4 $M_\odot$ and 10 km). Assuming the accretion disc to be truncated at the co-rotation radius, the observed mass accretion rate yields a maximum spin-up derivative of a few 10^{-13} Hz s^{-1}, fully consistent with the observed one.

A rough estimate of the NS dipolar magnetic field can be obtained by assuming the condition of spin equilibrium for the X-ray pulsar. The magnetic field can then be estimated as

$$B = 0.63\,\zeta^{-7/6} \left(\frac{P_{spin}}{2\,ms}\right)^{7/6} \left(\frac{M}{1.4\,M_\odot}\right)^{1/3} \left(\frac{\dot{M}}{10^{-10}\,M_\odot\,yr^{-1}}\right)^{1/2} 10^8\,G, \quad (1)$$

where ζ represents a model-dependent dimensionless factor (between 0.1 and 1) corresponding to the ratio between the magnetospheric radius and the Alfvén radius (see, e.g. Ghosh & Lamb 1979; Wang 1996), P_{spin} is the pulsar spin period in ms, and M is the NS mass. Assuming a 1.4 $M_\odot$ NS and the value of

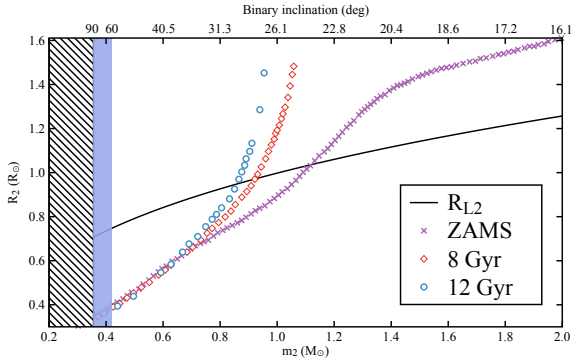

Fig. 5. Radius-mass plane showing the size constraints on the companion star Roche-lobe of IGR J17591–2342 (black solid line) obtained from the orbital parameters of the neutron star. The hatched region represents the constraints on the companion mass from the binary mass function, and the blue area defines the mass constraints for inclination angles between 60 and 90°. The other curves represent theoretical mass-radius relations for zero-age main-sequence stars (purple crosses) and isochrones for stars of 8 (red diamonds) and 12 Gyr (blue circles). The top x-axes represent the corresponding binary inclination angle in degrees assuming a 1.4 $M_\odot$.

$\dot{M}$ reported above, we obtain a range for the dipolar magnetic field of $1.4 \times 10^8 < B < 8 \times 10^9$ G, consistent with the average magnetic field of known AMXPs (see, e.g. Mukherjee et al. 2015).

With the NS mass function $f(m_2, m_1, i) \sim 1.5 \times 10^{-2}\, M_\odot$, we can constrain the mass of the companion star. Since neither total eclipses nor dips have been observed in the light curve, we can assume a binary inclination lower than 60° (see, e.g. Frank et al. 2002). As shown in Fig. 5, the upper limit on the inclination angle (represented in blue) allows us to limit the companion star mass $m_2 \gtrsim 0.42\, M_\odot$ (for a 1.4 $M_\odot$ NS), which increases up to $m_2 \gtrsim 0.52\, M_\odot$ if we consider a 2 $M_\odot$ NS. Introducing the contact condition ($R_2 \approx R_{L2}$) required to activate Roche-lobe overflow, we can express the donor radius as a function of its mass as $R_2 \simeq 0.87\, m_2^{1/3}\, P_{\rm orb,9\,h}^{2/3}\, R_\odot$, where m_2 is the companion mass in units of $M_\odot$ and $P_{\rm orb,9\,h}$ represents the binary orbital period in units of 9 h. In Fig. 5 we report the companion mass-radius relation (black solid line) assuming a 1.4 $M_\odot$ NS. For comparison, we show numerically simulated mass-radius relations for zero-age main-sequence stars (ZAMS; purple crosses; see, e.g. Tout et al. 1996), as well as isochrones for stars of 8 (red diamonds) and 12 Gyr (blue circles; see, e.g. Girardi et al. 2000). From the intersections with the mass-radius companion curve, we can infer that the donor is compatible with either a ZAMS with mass ∼1.1 $M_\odot$ (corresponding to an inclination angle of $i \sim 24°$) or an old main-sequence star with mass 0.85−0.92 $M_\odot$ (i ranging between 28 and 30°) for a stellar age between 8 and 12 Gyr. We note, however, that the a priori probability of observing a binary system with inclination $i \leq 30°$ is of the order of 13%. Mass values for which the main-sequence radius is smaller than the companion Roche lobe could still be acceptable if we consider the possibility of a bloated donor star. In that case, the thermal timescale (GM_2^2/R_2L_2) should be much longer than the evolutionary timescale ($M_2/\dot{M}_2$).

Finally, the broad-band energy spectrum of IGR J17591–2342 is well described by an absorbed soft black-body-like component ($kT \sim 0.8$ keV) with a relatively small emitting area that is compatible with emission from the neutron star surface (or part of it) plus a Comptonised component ($\Gamma \sim 1.8$) with a seed photon temperature compatible with the soft thermal component. The spectral properties of the source are consistent with those of other AMXPs observed in the hard state (see, e.g. Falanga et al. 2005; Gierliński & Poutanen 2005; Papitto et al. 2009, 2013; Sanna et al. 2017b,c). We found marginal evidence ($\Delta\chi^2 = 21$ for 2 d.o.f.) of a weak emission line that is compatible with the iron K-α transition. Even if marginally significant (an F-test gives a 4σ line significance), its introduction removes positive residuals around the expected energy, and such lines are not unusual for this type of source (see, e.g. Papitto et al. 2009, 2013; Sanna et al. 2017b,c). Table 2 shows that at later times, when the source re-brightens, the additional black body seems to disappear but the asymptotic Comptonisation power-law index increases. This might be due to more effective cooling of the seed photons by a thicker accretion stream above the stellar surface.

The discovery of another transient by INTEGRAL and its characterisation as the 22. accreting millisecond pulsar by *NuSTAR* and NICER enriches the census of these key objects in the understanding of the late stages of stellar evolution.

Acknowledgements. We thank Fiona Harrison for accepting a *NuSTAR* observation in the Director Discretionary Time. We thank the *Swift*, *NuSTAR*, and NICER teams for scheduling and performing these target-of-opportunity observations on short notice. This work was supported by NASA through the NICER and *NuSTAR* missions and the Astrophysics Explorers Program. It made use of data and software provided by the High Energy Astrophysics Science Archive Research Center (HEASARC). It is also based on observations with INTEGRAL, an ESA project with instruments and science data centre funded by ESA member states (especially the PI countries: Denmark, France, Germany, Italy, Switzerland, and Spain) and with the participation of Russia and the USA. DA acknowledges support from the Royal Society. LD acknowledges grant FKZ 50 OG 1602.

References

Alpar, M. A., Cheng, A. F., Ruderman, M. A., & Shaham, J. 1982, Nature, 300, 728
Altamirano, D., Casella, P., Patruno, A., Wijnands, R., & van der Klis, M. 2008, ApJ, 674, L45
Altamirano, D., Cavecchi, Y., Patruno, A., et al. 2011, ApJ, 727, L18
Arnaud, K. A. 1996, ASP Conf. Ser., 101, 17
Bozzo, E., Ducci, L., Ferrigno, C. et al. 2018, ATel, 11942
Burderi, L., & Di Salvo, T. 2013, Mem. Soc. Astron. It., 84, 117
Campana, S., & Di Salvo, T. 2018, ArXiv e-prints [arXiv:1804.03422]
Casella, P., Altamirano, D., Patruno, A., Wijnands, R., & van der Klis, M. 2008, ApJ, 674, L41
Ducci, L., Kuulkers, E., Grinberg, V., et al. 2018, ATel, 11941
Falanga, M., Bonnet-Bidaud, J. M., Poutanen, J., et al. 2005, A&A, 436, 647
Ferrigno, C., Bozzo, E., Falanga, M., et al. 2011, A&A, 525, A48
Frank, J. , King, A. R. , & Raine, D. J. 2002, Accretion Power in Astrophysics, 3rd edn. (Cambridge University Press)
Ghosh, P., & Lamb, F. K. 1979, ApJ, 232, 259
Gierliński, M., & Poutanen, J. 2005, MNRAS, 359, 1261
Girardi, L., Bressan, A., Bertelli, G., & Chiosi, C. 2000, A&AS, 141, 371
Kaastra, J. S., & Bleeker, J. A. M. 2016, A&A, 587, A151
Kerr, F. J., & Lynden-Bell, D. 1986, MNRAS, 221, 1023
Krimm, H. A., Barthelmy, S. D., & Cummings, J. R. 2018, ATel, 11981
Madsen, K. K., Harrison, F. A., Markwardt, C. B., et al. 2015, ApJS, 220, 8
Markwardt, C. B., & Strohmayer, T. E. 2010, ApJ, 717, L149
Mukherjee, D., Bult, P., van der Klis, M., & Bhattacharya, D. 2015, MNRAS, 452, 3994
Nowak, M. A., Paizis, A., & Chenevez, J. et al. 2018, ATel, 11988
Papitto, A., Di Salvo, T., D'Aì, A., et al. 2009, A&A, 493, L39
Papitto, A., D'Aì, A., Di Salvo, T., et al. 2013, MNRAS, 429, 3411
Patruno, A., & Watts, A. L. 2012, ArXiv e-prints [arXiv:1206.2727]
Romano, P., Campana, S., Chincarini, G., et al. 2006, A&A, 456, 917
Russell, T., Degenaar, N., Wijnands, R., & van den Eijnden, J. 2018, ATel, 11954
Sanna, A., Burderi, L., Riggio, A., et al. 2016, MNRAS, 459, 1340
Sanna, A., Di Salvo, T., Burderi, L., et al. 2017a, MNRAS, 471, 463
Sanna, A., Papitto, A., Burderi, L., et al. 2017b, A&A, 598, A34
Sanna, A., Pintore, F., Bozzo, E., et al. 2017c, MNRAS, 466, 2910
Tout, C. A., Pols, O. R., Eggleton, P. P., & Han, Z. 1996, MNRAS, 281, 257
Wang, Y.-M. 1996, ApJ, 465, L111
Welsh, W. F., Robinson, E. L., & Young, P. 2000, AJ, 120, 943